Int. J. Dynam. Control
DOI 10.1007/s40435-017-0331-9

Retarded, neutral and advanced differential equation models for balancing using an accelerometer

Balazs A. Kovacs[1] · **Tamas Insperger**[1]

Received: 21 March 2017 / Revised: 27 April 2017 / Accepted: 29 April 2017

Abstract Stabilization of a pinned pendulum about its upright position via a reaction wheel is considered, where the pendulum's angular position is measured by a single accelerometer attached directly to the pendulum. The control policy is modeled as a simple PD controller and different feedback mechanisms are investigated. It is shown that depending on the modeling concepts, the governing equations can be a retarded functional differential equation or neutral functional differential equation or even advanced functional differential equation. These types of equations have radically different stability properties. In the retarded and the neutral case the system can be stabilized, but the advanced equations are always unstable with infinitely many unstable characteristic roots. It is shown that slight modeling differences lead to significant qualitative change in the behavior of the system, which is demonstrated by means of the stability diagrams for the different models. It is concluded that digital effects, such as sampling, stabilizes the system independently on the modeling details.

Keywords Feedback delay · Accelerometer · Functional differential equations · Semi-discretization · D-subdivision method · Stabilization

✉ Tamas Insperger
insperger@mm.bme.hu

Balazs A. Kovacs
balazs.kovacs@mm.bme.hu

[1] Department of Applied Mechanics, Budapest University of Technology and Economics and MTA-BME Lendület Human Balancing Research Group, Budapest, Hungary

1 Introduction

Functional differential equations (FDEs) describes systems, where the rate of change of the state depends on the state at deviating arguments. Typically these equations can be categorized into three groups [1,2]. (1) If the rate of change of the state depends on the past state of the system, then the corresponding mathematical model is a *retarded functional differential equation* (*RFDE*). (2) If the rate of change of the state depends on the past values of both the state and its rate of change then the governing equation is called *neutral functional differential equation* (*NFDE*). (3) If the rate of change of the state depends on the past values of higher derivatives of the state then the system is described by an *advanced functional differential equations* (*AFDEs*). A possible representation of these equations is

$$\dot{\mathbf{x}}(t) = \mathbf{f}(\mathbf{x}(t), \mathbf{x}(t-\tau), \dot{\mathbf{x}}(t-\tau), \ddot{\mathbf{x}}(t-\tau)), \tag{1}$$

where $\mathbf{x} \in \mathbb{R}^n$ is the state variable and τ is the time delay.

While retarded and neutral FDEs are often used to model different phenomena in engineering and physics, advanced FDEs rarely show up in engineering applications due to their inverted causality, which can be demonstrated by the following example. Consider the simple scalar AFDE

$$\dot{x}(t) = \ddot{x}(t-\tau). \tag{2}$$

Here, the change of rate of the state (say velocity) at time instant t depends on the second derivate of the state (say acceleration) at time instant $t-\tau$. By a time-shift transformation $\tilde{t} = t - \tau$ and by introducing a new variable $z(t) = \dot{x}(t)$ the equation can be written in the following form

$$z'(\tilde{t}) = z(\tilde{t} + \tau), \tag{3}$$

Published online: 17 May 2017

where $'$ stands for derivation with respect to $\tilde{t}$. Thus, the rate of change of state is determined by the future values of the state, which explains the terminology *advanced*.

While stability properties of RFDEs and NFDEs depend on the system and control parameters, AFDEs are always unstable with infinitely many unstable characteristic roots [3,4]. Therefore real physical problems are usually described by RFDEs or NFDEs (see, e.g., Xu et al. [5], [6]). For instance, if the displacement and the velocity is fed back with a delay in a second-order system, then the governing equation is a RFDE [7,8]. If the acceleration is also fed back with delay, then one obtain a NFDE. In the case when the jerk (the first derivative of the acceleration) is fed back with delay, then the governing equation becomes an AFDE.

In this paper, a balancing task is modelled using different concepts resulting in a variety of governing equations involving RFDEs, NFDEs and AFDEs. The model under investigation is originated from the model used in [9]. Namely, it is assumed that the angular position of the balanced body is measured by an accelerometer. However, as opposed to the model in [9], where a static model of the accelerometer was used, here we model the accelerometer as an oscillator. Both continuous-time (analogue) and discrete-time (digital) feedback mechanisms are investigated for different sampling concepts and it is shown that discrete-time sampling has major effect on the stability properties. The different models are compared by means of stability diagrams.

2 Mechanical models

A simple mechanical model of balancing tasks is shown in Fig. 1. The body to be balanced is pinned at point O and a control torque Q is provided by a reaction wheel (also called inertial wheel) connected to the body at point B. The reaction wheel is driven by a DC motor, whose torque is assumed to be controlled directly. Due to the action-reaction effect, this mechanism can be used to apply a control torque on the body (see, e.g., [10]). The angular position φ of the body versus vertical is measured by an accelerometer, which is modelled as a spring-mass system, attached to the body at point A. The output signal y of the accelerometer, which is used as input in the controller, is assumed to be proportional to the relative displacement ξ of the block of mass m_0 in the piezo-ceramic crystal such that

$$y = K_{\mathrm{a}}\xi, \tag{4}$$

where K_{a} [V/m] is the characteristic constant of the accelerometer. The control mechanism is realized with a simple PD controller. It is assumed that the angular position and the angular velocity of the reaction wheel is not controlled. The linearized equations of motion reads

$$\left(J_{\mathrm{o}} + m_0 a^2\right)\ddot{\varphi}(t) + m_0 a\ddot{\xi}(t) - (mgH - m_0 ga)\,\varphi(t) - m_0 g\xi(t) = Q(t), \tag{5}$$

$$m_0 a\ddot{\varphi}(t) + m_0\ddot{\xi}(t) + k_0\dot{\xi}(t) - m_0 g\varphi(t) + s_0\xi(t) = 0, \tag{6}$$

where m is the mass of the body, H is the distance between the center of gravity C and the pivot point O, J_{o} is the mass moment of inertia with respect to the axis o normal to the plane of the figure through point O of the pendulum, m_0, s_0 and k_0 are the modal mass, the stiffness, and the damping parameters of the accelerometer and a is the distance between the suspension point O and the accelerometer. The parameters of the body are fixed to $H = 0.2$ m, $m = 0.5$ kg and $J_{\mathrm{o}} = 0.2\,\mathrm{kg\,m^2}$. The modal mass and stiffness parameters of the accelerometer are taken from [11], as $m_0 = 9.65 \times 10^{-7}$ kg and $s_0 = 141$ N/m, while the damping parameter is set to $k_0 = 0.01$ Ns/m. The parameters m, H, J_{o}, m_0, s_0 and k_0 are fixed during the study, while the different values of a are investigated.

The control torque Q is calculated using the output y of the accelerometer according to the PD feedback scheme $Q = Py + D\dot{y}$, where P and D are the proportional and the derivative control gains. The idea behind this feedback is that, in case of a fixed position $\varphi \equiv \varphi^*$ with $\varphi^* \neq 0$ and $|\varphi^*|$ being small, the displacement ξ and therefore the output y are proportional to the angular position φ. Four different concepts are considered for the calculation of the control torque Q.

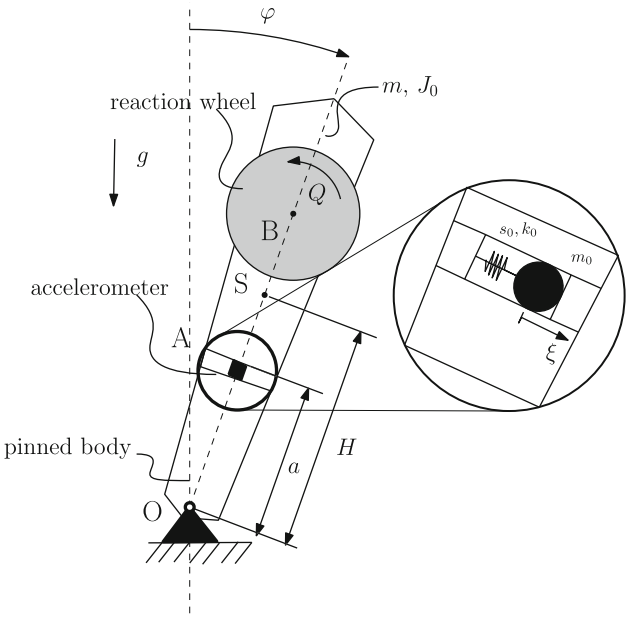

Fig. 1 Mechanical model: the pinned body, the accelerometer and the reaction wheel

(C1) Real-time analogue control:

$$Q(t) = P\, y(t) + D\, \dot{y}(t). \tag{7}$$

(C2) Analogue control with a constant feedback delay τ:

$$Q(t) = P\, y(t-\tau) + D\, \dot{y}(t-\tau). \tag{8}$$

(C3) Discrete-time control with sampling period h and with feedback delay:

$$Q(t) = P\, y(t_{j-r}) + D\, \dot{y}(t_{j-r}), \quad t \in [t_j, t_{j+1}), \quad t_j = jh, \quad j \in \mathbb{Z}^+. \tag{9}$$

Here $r \in \mathbb{N}$ is the delay parameter and $\tau = rh$ is the feedback delay.

(C4) Discrete-time control with numerically calculated derivative term:

$$Q(t) = P\, y(t_{j-r}) + D\, \frac{y(t_{j-r}) - y(t_{j-r-1})}{h}, \quad t \in [t_j, t_{j+1}), \quad t_j = jh, \quad j \in \mathbb{Z}^+. \tag{10}$$

The fact that the characteristic time constant of the accelerometer ($1/\sqrt{s_0/m_0}$) is smaller by a factor of 5000 than that of the pinned body ($1/\sqrt{mgH/J_o}$) implies that the dynamic effect of the accelerometer can be neglected. Based on this concept, we consider four different models by neglecting terms involving the dynamic parameters of the accelerometer.

(M1) In a quasi-static model, we assume that all the terms involving m_0 and k_0 are negligible except for the static term $m_0 g\varphi(t)$ in Eq. (6). In this case Eq. (5) can be simplified to

$$J_o\ddot{\varphi}(t) - mgH\varphi(t) = Q(t), \tag{11}$$

while Eq. (6) gives

$$\xi(t) = \frac{m_0 g}{s_0}\varphi(t). \tag{12}$$

This model with control concepts C1, C2, C3 and C4 gives respectively the models 1.0, 1.1, 1.2 and 1.3 analyzed in [9].

(M2) In a semi-quasi-static model, we assume that again all the terms involving m_0 and k_0 are negligible except for two terms, namely, the static term $m_0 g\varphi(t)$ and the dynamic term $m_0 a\ddot{\varphi}(t)$ in Eq. (6). The corresponding equation of motion is the same as (11), but the displacement ξ can now be given as a linear combination of the angular displacement and angular acceleration as

$$\xi(t) = \frac{m_0 g}{s_0}\varphi(t) - \frac{m_0 a}{s_0}\ddot{\varphi}(t). \tag{13}$$

This model gives cases 2.0, 2.1, 2.2 and 2.3 in [9]. The combination of model M2 with control force models C2 and C3 results in an AFDE and in an NFDE, respectively. For more details on these models, see [9]. Note that if $a = 0$ then models M1 and M2 are identical.

(M3) An extension of model M2 is that only the term $m_0\ddot{\xi}(t)$ is neglected in Eq. (6), and the term $k_0\dot{\xi}(t)$ is left unchanged. In this case the system is governed by Eq. (11) together with

$$m_0 a\ddot{\varphi}(t) + k_0\dot{\xi}(t) - m_0 g\varphi(t) + s_0\xi(t) = 0, \tag{14}$$

This model corresponds to a 1.5-degree-of-freedom dynamical system, since only the first derivative of the state variable $\xi(t)$ shows up in the governing equations. Although the validity of this model might be questionable, it provides a transition between model M2 and model M4 with some interesting features.

(M4) No terms are neglected in Eqs. (5) and (6). This model corresponds to a 2-degree-of-freedom dynamical system with generalized coordinates φ and ξ.

Models M1 and M2 were already analyzed in details in [9]. Here, we extend the analysis by models M3 and M4, which together with the four models of the control force give eight different cases. Different models are named by combining the above notations. For instance, M3C1 refers to mechanical model M3 with control force model C1.

3 Analysis of the different models

In this section all combinations of the mechanical models and control concepts listed in Sect. 2 are discussed and their stability properties are investigated by means of stability charts. The equations of motion is written in the state space form

$$\dot{\mathbf{x}}(t) = \mathbf{A}\mathbf{x}(t) + \mathbf{B}Q(t), \tag{15}$$

where the state variable $\mathbf{x}$ and the matrices $\mathbf{A}$ and $\mathbf{B}$ is given for the individual model combinations.

3.1 Mechanical model M1

In this model, the system is governed by (15) with

$$\mathbf{x} = \begin{bmatrix} \varphi \\ \dot{\varphi} \end{bmatrix}, \quad \mathbf{A} = \begin{bmatrix} 0 & 1 \\ b & 0 \end{bmatrix}, \quad \mathbf{B} = \begin{bmatrix} 0 \\ B \end{bmatrix}, \tag{16}$$

where $B = 1/J_\mathrm{o}$ and

$$b = \frac{mgH}{J_\mathrm{o}} = 4.905\,\frac{1}{\mathrm{s}^2} \tag{17}$$

is the system parameter. The output signal of the acceleration can be given using (4) and (12) as

$$y = \frac{K_\mathrm{a} m_0 g}{s_0}\varphi. \tag{18}$$

Since model M1 is a special case of model M2, the properties associated with different control models are not detailed here.

3.2 Mechanical model M2

This model is governed by (15) with **A** and **B** given in (16) as in model M1, but here the output of the acceleration is determined by (4) and (13), which give

$$y = \frac{K_\mathrm{a} m_0 g}{s_0}\varphi - \frac{K_\mathrm{a} m_0 a}{s_0}\ddot{\varphi}. \tag{19}$$

The special case $a = 0$ gives model M1.

3.2.1 Model M2C1

In model M2C1, the acceleration signal y and its derivative $\dot{y}$ are fed back without any delay. Consequently, the control torque can be given as

$$Q(t) = \mathbf{K}(\mathbf{x}(t) - \varepsilon\ddot{\mathbf{x}}(t)), \tag{20}$$

where

$$\varepsilon = \frac{a}{g} \tag{21}$$

is a parameter proportional to distance a between the suspension point and the accelerometer and

$$\mathbf{K} = \begin{bmatrix} -p & -d \end{bmatrix} \tag{22}$$

with

$$p = \frac{K_\mathrm{a} m_0 g}{s_0}\,P, \quad d = \frac{K_\mathrm{a} m_0 g}{s_0}\,D. \tag{23}$$

The characteristic equation of the system can be written in the form

$$D(\lambda) = -\varepsilon d\lambda^3 + (1-\varepsilon p)\lambda^2 + d\lambda + (p-b) = 0. \tag{24}$$

If $\varepsilon \neq 0$, then the system is unstable independently of the other parameters. If $\varepsilon = 0$ (this case give model M1C1), then the system is asymptotically stable if and only $d > 0$ and $p > b$.

3.2.2 Model M2C2

In case of model M2C2, the delay of the feedback loop is also involved into the model, and the control torque has the form

$$Q(t) = \mathbf{K}(\mathbf{x}(t-\tau) - \varepsilon\ddot{\mathbf{x}}(t-\tau)), \tag{25}$$

The characteristic equation in this case reads

$$\begin{aligned} D(\lambda) = &-\varepsilon d\mathrm{e}^{-\lambda\tau}\lambda^3 + (1-\varepsilon p\mathrm{e}^{-\lambda\tau})\lambda^2 + d\mathrm{e}^{-\lambda\tau}\lambda \\ &+ (p\mathrm{e}^{-\lambda\tau} - b) = 0. \end{aligned} \tag{26}$$

The case $\varepsilon = 0$ gives model M1C2, which is the basic equation for balancing problems in the presence of feedback delay [12]. The stability regions in the plane (p, d) are bounded by the line $p = b$ and the parametric curve

$$p = (\omega^2 + b)\cos\omega\tau, \quad d = \frac{(\omega^2+b)}{\omega}\sin\omega\tau, \tag{27}$$

with $\omega \in \mathbb{R}^+$. The corresponding stability charts can be seen in Fig. 2 with $\tau = 0.2$ s. It is known that this system is always unstable if the system parameter b is larger than the critical value $b_\mathrm{crit} = 2/\tau^2$ (see [13]).

If $\varepsilon \neq 0$ (the case of M2C2), then the highest derivative appears with a delayed argument, thus the governing equation is an autonomous AFDE. Consequently this system is always unstable with infinitely many unstable roots (number of unstable roots, NUR $= \infty$), if $\varepsilon d \neq 0$.

3.2.3 Model M2C3

In engineering applications, feedback loops are typically implemented using digital controllers [14–16]. In this case, the system is governed by (15) with (9). Due to the piecewise-constant forcing, this system can be solved as an ODE over a sampling interval $[t_j, t_{j+1})$ and, if $r \geq 1$, a finite-dimensional discrete map can be constructed in the form

$$\begin{bmatrix} \mathbf{x}_{j+1} \\ \ddot{\mathbf{x}}_{j+1} \\ Q_j \\ Q_{j-1} \\ \vdots \\ Q_{j-r+1} \end{bmatrix} = \underbrace{\begin{bmatrix} \mathbf{P} & \mathbf{0}_{2\times2} & \mathbf{0}_{2\times1} & \dots & \mathbf{0}_{2\times1} & \mathbf{RB} \\ \mathbf{A}^2\mathbf{P} & \mathbf{0}_{2\times2} & \mathbf{0}_{2\times1} & \dots & \mathbf{0}_{2\times1} & \mathbf{SB} \\ \mathbf{K} & -\varepsilon\mathbf{K} & 0 & \dots & 0 & 0 \\ \mathbf{0}_{1\times2} & \mathbf{0}_{1\times2} & 1 & & 0 & 0 \\ \vdots & \vdots & & \ddots & & \vdots \\ \mathbf{0}_{1\times2} & \mathbf{0}_{1\times2} & 0 & \dots & 1 & 0 \end{bmatrix}}_{\mathbf{\Phi}_\mathrm{M2C3}} \begin{bmatrix} \mathbf{x}_j \\ \ddot{\mathbf{x}}_j \\ Q_{j-1} \\ Q_{j-2} \\ \vdots \\ Q_{j-r} \end{bmatrix} \tag{28}$$

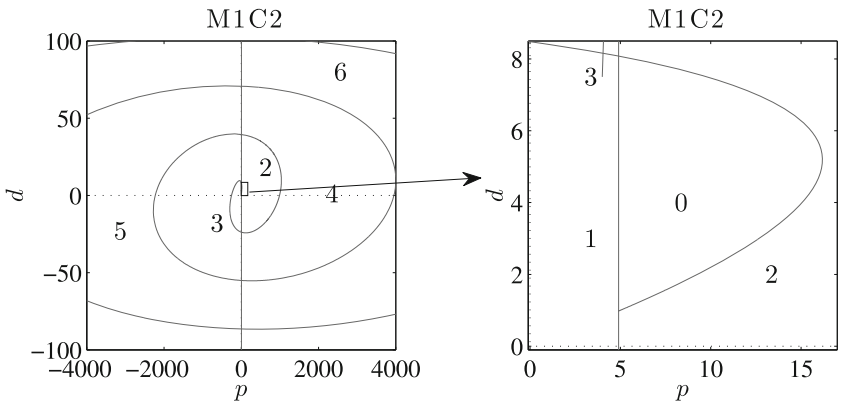

Fig. 2 Stability boundaries and the number of unstable roots (NUR) for M1C2

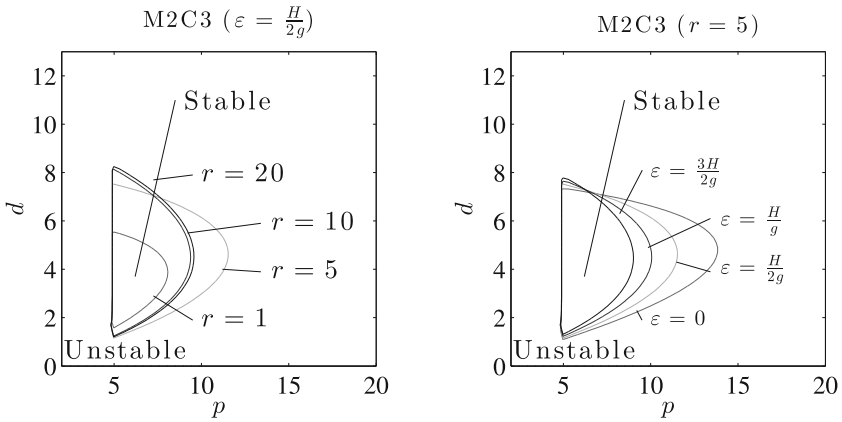

Fig. 3 Stability boundaries for M1C3 ($\varepsilon = 0$) and M2C3 $\left(\varepsilon = \frac{H}{2g}\right)$ with $\tau = 0.2$ s

where $\mathbf{x}_j = \mathbf{x}(t_j)$, $\ddot{\mathbf{x}}_j = \ddot{\mathbf{x}}(t_j)$, $Q_j = Q(t_j)$,

$$\mathbf{P} = \mathrm{e}^{\mathbf{A}h}, \quad \mathbf{R} = \int_0^h \mathrm{e}^{\mathbf{A}(h-s)}\mathrm{d}s,$$
$$\mathbf{S} = \int_0^h \mathbf{A}^2\mathrm{e}^{\mathbf{A}(h-s)}\mathrm{d}s + \mathbf{A}, \tag{29}$$

and $\mathbf{0}_{n\times m}$ is a $n \times m$ zero matrix with $n, m \in \mathbb{Z}^+$. This discrete map corresponds to the semidiscretization of model M2C2 [12]. The stability of the system can be defined by the eigenvalues of the monodromy matrix $\mathbf{\Phi}_{\mathrm{M2C3}}$ in (28). The system is asymptotically stable if all the eigenvalues are in modulus less than one. Some sample stability charts are presented in Fig. 3 for different ε, and for different r parameters.

3.2.4 Model M2C4

In this case, the system is governed by (15) with (10). Similarly to model M2C3, the solution can be given over a sampling interval $[t_j, t_{j+1})$, and, if $r \geq 1$, a finite-dimensional discrete map can be constructed in the form

$$\begin{bmatrix} \mathbf{x}_{j+1} \\ \ddot{\mathbf{x}}_{j+1} \\ Q_j \\ Q_{j-1} \\ \vdots \\ Q_{j-r} \end{bmatrix} = \underbrace{\begin{bmatrix} \mathbf{P} & \mathbf{0}_{2\times 2} & \mathbf{0}_{2\times 1} & \dots & \mathbf{R}\mathbf{B}K_1 & \mathbf{R}\mathbf{B}K_2 \\ \mathbf{A}^2\mathbf{P} & \mathbf{0}_{2\times 2} & \mathbf{0}_{2\times 1} & \dots & \mathbf{S}\mathbf{B}K_1 & \mathbf{S}\mathbf{B}K_2 \\ \mathbf{C}_2 & -\varepsilon\mathbf{C}_2 & 0 & \dots & 0 & 0 \\ \mathbf{0}_{1\times 2} & \mathbf{0}_{1\times 2} & 1 & \dots & 0 & 0 \\ \vdots & & & \ddots & & \vdots \\ \mathbf{0}_{1\times 2} & \mathbf{0}_{1\times 2} & 0 & \dots & 1 & 0 \end{bmatrix}}_{\mathbf{\Phi}_{\mathrm{M2C4}}} \begin{bmatrix} \mathbf{x}_j \\ \ddot{\mathbf{x}}_j \\ Q_{j-1} \\ Q_{j-2} \\ \vdots \\ Q_{j-r-1} \end{bmatrix}, \tag{30}$$

where $Q_j = \varphi(t_j) - \varepsilon\ddot{\varphi}(t_j)$, $\mathbf{P}, \mathbf{R}, \mathbf{S}$ are defined in (29) and

$$\mathbf{C}_2 = \begin{bmatrix} 1 & 0 \end{bmatrix}, \quad K_1 = -\frac{p+d}{h}, \quad K_2 = \frac{d}{h}. \tag{31}$$

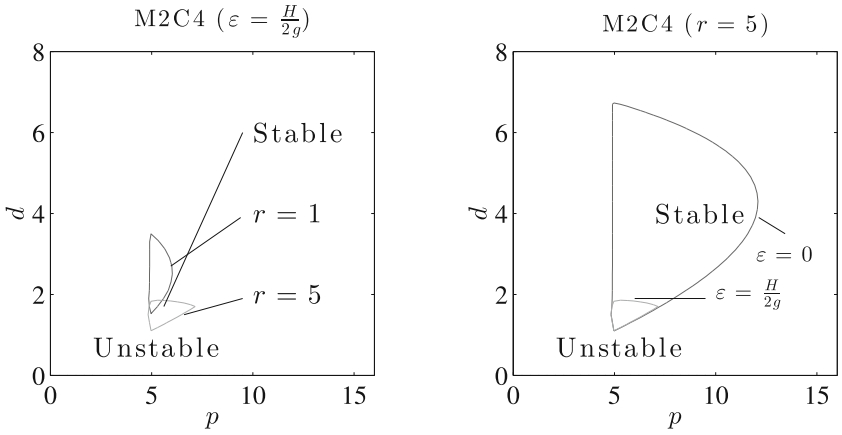

Fig. 4 Stability boundaries for M1C4 ($\varepsilon = 0$) and M2C4 $\left(\varepsilon = \frac{H}{2g}\right)$ with $\tau = 0.2\,\mathrm{s}$

The stability of the system can be defined by the eigenvalues of the monodromy matrix $\mathbf{\Phi}_{\mathrm{M2C4}}$ in (30). Some sample stability charts are presented in Fig. 4 for different ε, and for different r parameters.

3.3 Mechanical model M3

Equation (11) with (14) can be written in the state space form of (15) with

$$\mathbf{x} = \begin{bmatrix} \varphi \\ \dot{\varphi} \\ \xi \end{bmatrix}, \quad \mathbf{A} = \begin{bmatrix} 0 & 1 & 0 \\ b & 0 & 0 \\ \frac{m_0(g-ab)}{k_0} & 0 & -\frac{s_0}{k_0} \end{bmatrix},$$

$$\mathbf{B} = \begin{bmatrix} 0 \\ B \\ -\frac{m_0 a B}{k_0} \end{bmatrix}. \tag{32}$$

This model corresponds to a 1.5-degree-of-freedom dynamical system. The output of the accelerometer is given by (4), which is used as input for the different control torque models.

3.3.1 Model M3C1

Equation (15) with (32), (7) and (4) yields the characteristic equation of form

$$D(\lambda) = \left(1 - \frac{m_0 a B d}{k_0}\right)\lambda^3 + \left(\frac{s_0}{k_0} - \frac{m_0 a B p}{k_0}\right)\lambda^2 + \left(\frac{m_0 g B d}{k_0} - b\right)\lambda + \left(\frac{m_0 g B p}{k_0} - b\frac{s_0}{k_0}\right) = 0. \tag{33}$$

It can easily be see that this system is unstable for any control gain parameters p and d.

3.3.2 Model M3C2

Equation (15) with (32), (8) and (4) gives a system of NFDEs. The associated characteristic equation reads

$$D(\lambda) = \left(1 - \frac{m_0 a B d}{k_0}\,\mathrm{e}^{-\lambda\tau}\right)\lambda^3 + \left(\frac{s_0}{k_0} - \frac{m_0 a B p}{k_0}\,\mathrm{e}^{-\lambda\tau}\right)\lambda^2 + \left(\frac{m_0 g B d}{k_0}\,\mathrm{e}^{-\lambda\tau} - b\right)\lambda + \left(\frac{m_0 g B p}{k_0}\,\mathrm{e}^{-\lambda\tau} - b\frac{s_0}{k_0}\right) = 0. \tag{34}$$

The so-called D-curves, which separate the regions with different NUR in the plane (p, d), are the line $p = Hms_0/(m_0)$ and the parametric curve

$$p = \frac{(\omega^2 + b)(s_0 \cos\omega\tau - k_0\omega \sin\omega\tau)}{B m_0 (g + a\omega^2)}, \tag{35}$$

$$d = \frac{(\omega^2 + b)(k_0\omega \cos\omega\tau + s_0 \sin\omega\tau)}{B m_0 \omega (g + a\omega^2)} \tag{36}$$

with $\omega \in \mathbb{R}^+$. Note that this system is always unstable with NUR$= \infty$ if $1 < |m_0 a B d/k_0|$. If $1 > |m_0 a B d/k_0|$, then the system can be stabilized by a properly chosen pair (p, d). A sample stability chart can be seen in Fig. 5, which shows the D-curves for $\varepsilon = a/g = 3 \times 10^{-5}$ 1/s and for $\tau = 0.2$ s. It can be shown that the system has infinitely many unstable roots if $d > |k_0 J_\mathrm{o}/(m_0 a)|$ and it has finite NUR if $d < |k_0 J_\mathrm{o}/(m_0 a)|$.

3.3.3 Model M3C3

Piecewise solution of Eq. (15) with (32), (9) and (4) over a sampling period gives the finite dimensional discrete map

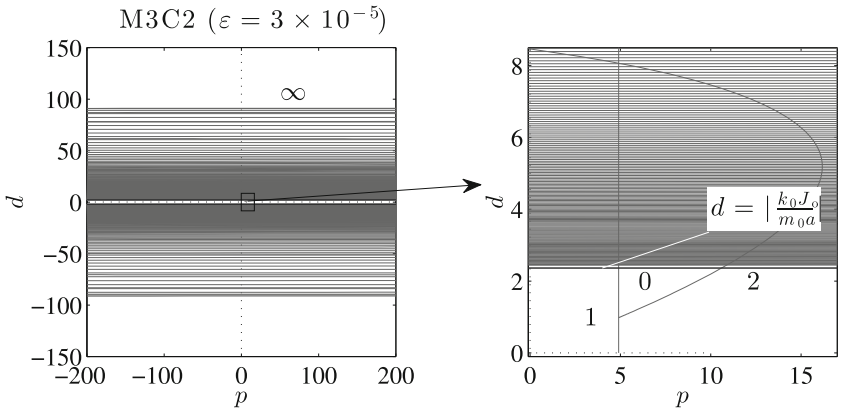

Fig. 5 D-curves and the NURs for M3C2 with $\tau = 0.2$ s

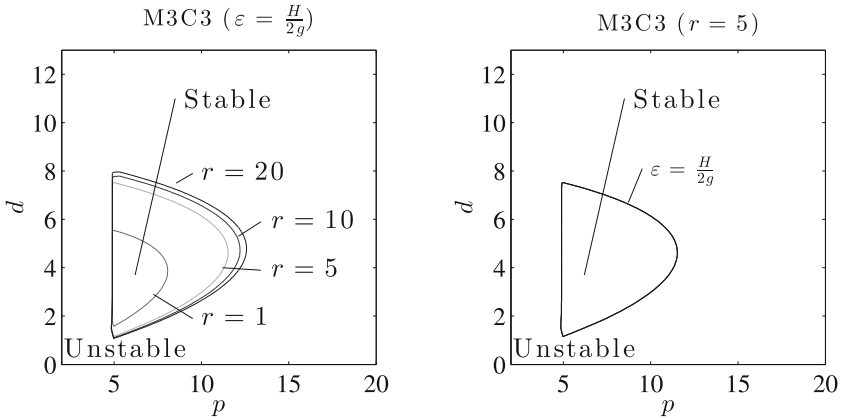

Fig. 6 Stability boundaries for M3C3 with $\tau = 0.2$ s

$$\begin{bmatrix} \mathbf{x}_{j+1} \\ \dot{\mathbf{x}}_{j+1} \\ Q_j \\ Q_{j-1} \\ \vdots \\ Q_{j-r+1} \end{bmatrix} = \underbrace{\begin{bmatrix} \mathbf{P} & \mathbf{0}_{3\times3} & \mathbf{0}_{3\times1} & \dots & \mathbf{0}_{3\times1} & \mathbf{RB} \\ \mathbf{AP} & \mathbf{0}_{3\times3} & \mathbf{0}_{3\times1} & \dots & \mathbf{0}_{3\times1} & \mathbf{TB} \\ -p\mathbf{C}_3 & -d\mathbf{C}_3 & 0 & \dots & 0 & 0 \\ \mathbf{0}_{1\times3} & \mathbf{0}_{1\times3} & 1 & \dots & 0 & 0 \\ \vdots & \vdots & & \ddots & & \vdots \\ \mathbf{0}_{1\times3} & \mathbf{0}_{1\times3} & 0 & \dots & 1 & 0 \end{bmatrix}}_{\mathbf{\Phi}_{\text{M3C3}}} \begin{bmatrix} \mathbf{x}_j \\ \dot{\mathbf{x}}_j \\ Q_{j-1} \\ Q_{j-2} \\ \vdots \\ Q_{j-r} \end{bmatrix} \tag{37}$$

where $\mathbf{P}$ and $\mathbf{R}$ are defined in (29) with (32) and

$$\mathbf{T} = \int_0^h \mathbf{A}e^{\mathbf{A}(h-s)}ds + \mathbf{I}, \qquad \mathbf{C}_3 = \begin{bmatrix} 0 & 0 & 1 \end{bmatrix}. \tag{38}$$

The stability of the system is determined by the eigenvalues of the monodromy matrix $\mathbf{\Phi}_{\text{M3C3}}$ in (37). The system is asymptotically stable if all the eigenvalues are in modulus less than one. Some sample stability charts are presented in Fig. 6 for different ε and for different r parameters.

Model M3C4

Equation (15) with (32), (10) and $r \geq 1$ generates the discrete map

$$\begin{bmatrix} \mathbf{x}_{j+1} \\ Q_j \\ Q_{j-1} \\ \vdots \\ Q_{j-r} \end{bmatrix} = \underbrace{\begin{bmatrix} \mathbf{P} & \mathbf{0}_{3\times1} & \dots & \mathbf{RB}K_1 & \mathbf{RB}K_2 \\ \mathbf{C}_3 & 0 & \dots & 0 & 0 \\ \mathbf{0}_{1\times3} & 1 & \dots & 0 & 0 \\ \vdots & & \ddots & & \vdots \\ \mathbf{0}_{1\times3} & 0 & \dots & 1 & 0 \end{bmatrix}}_{\mathbf{\Phi}_{\text{M3C4}}} \begin{bmatrix} \mathbf{x}_j \\ Q_{j-1} \\ Q_{j-2} \\ \vdots \\ Q_{j-r-1} \end{bmatrix}, \tag{39}$$

where $\mathbf{P}$ and $\mathbf{R}$ are defined in (29) with (32), and K_1 and K_2 are defined in (31). The stability of the system is determined by the eigenvalues of the monodromy matrix $\mathbf{\Phi}_{\text{M3C4}}$ in (39).

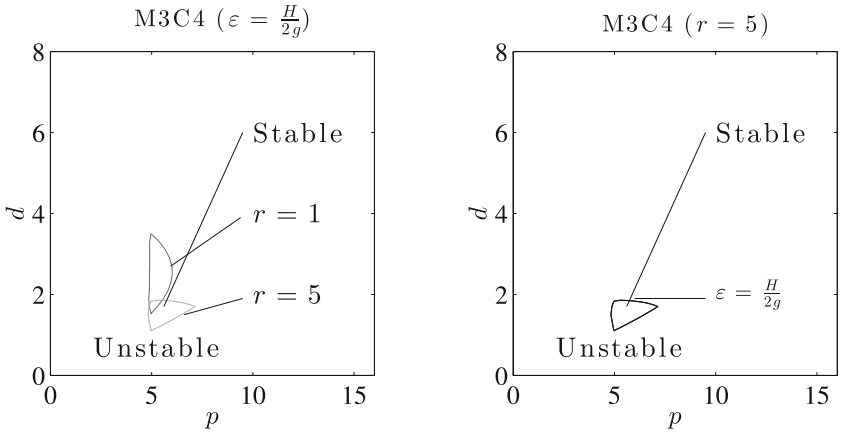

Fig. 7 Stability boundaries for M3C4 with $\tau = 0.2$ s

The stability charts are presented on Fig. 7 for different ε and for different r parameters.

3.4 Mechanical model M4

The full dynamics of the system shown in Fig. 1 can be modeled as a 2-degree-of-freedom system. Equations (5) and (6) can be written in the form of (15) with

$$\mathbf{x} = \begin{bmatrix} \varphi \\ \xi \\ \dot{\varphi} \\ \dot{\xi} \end{bmatrix}, \quad \mathbf{B} = \begin{bmatrix} 0 \\ 0 \\ B \\ -m_0 a B \end{bmatrix}, \tag{40}$$

and

$$\mathbf{A} = \begin{bmatrix} 0 & 0 & 1 & 0 \\ 0 & 0 & 0 & 1 \\ b & B(gm_0 + as_0) & 0 & aBk_0 \\ (g-ab)m_0 & -aBm_0(gm_0 + as_0) - s_0 & 0 & -k_0(a^2 Bm_0 + 1) \end{bmatrix}. \tag{41}$$

3.4.1 Model M4C1

Equation (15) with (40–41) and (7) with (4) yields the characteristic equation of form

$$\begin{aligned} D(\lambda) = \lambda^4 &+ \left(\frac{k_0}{m_0} + aBd + a^2 Bk_0\right)\lambda^3 \\ &+ \left(aBgm_0 + a^2 Bs_0 + \frac{s_0}{m_0} + aBp - b\right)\lambda^2 \\ &- \left(aBgk_0 + Bgd + b\frac{k_0}{m_0}\right)\lambda \\ &- \left(Bgp + Bg^2 m_0 + aBgs_0 + b\frac{s_0}{m_0}\right) = 0. \end{aligned} \tag{42}$$

It can be shown using the Routh–Hurwitz criteria that this system cannot be stabilized with any control parameters, similarly to model M3C1.

3.4.2 Model M4C2

When the feedback delay is also involved into the model, then Eq. (15) with (40–41) and (8) with (4) gives a system of RFDEs. The associated characteristic equation has the form

$$\begin{aligned} D(\lambda) = \lambda^4 &+ \left(\frac{k_0}{m_0} + aBde^{-\lambda\tau} + a^2 Bk_0\right)\lambda^3 \\ &+ \left(aBgm_0 + a^2 Bs_0 + \frac{s_0}{m_0} + aBpe^{-\lambda\tau} - b\right)\lambda^2 \\ &- \left(aBgk_0 + Bgde^{-\lambda\tau} + b\frac{k_0}{m_0}\right)\lambda \\ &- \left(Bgpe^{-\lambda\tau} + Bg^2 m_0 + aBgs_0 + b\frac{s_0}{m_0}\right) = 0. \end{aligned} \tag{43}$$

The D-curves separating the regions with different NUR in the plane (p, d) are the line $p = mHs_0/m_0 + m_0 g + as_0$ and the parametric curve

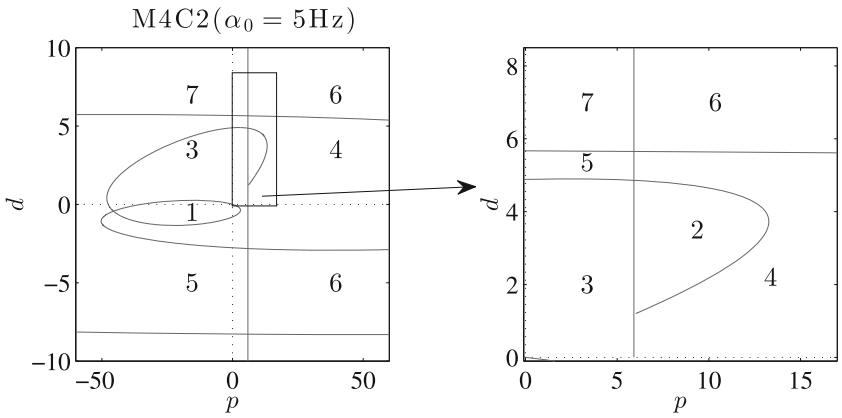

Fig. 8 Stability boundaries and the number of unstable roots (NUR) for M3C2 with $\tau = 0.2$ s, $\alpha_0 = 5$ Hz

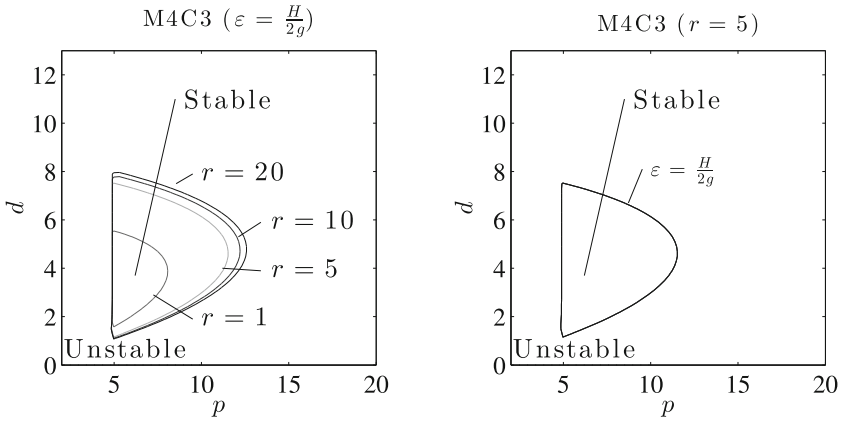

Fig. 9 Stability boundaries for M4C3 with $\tau = 0.2$ s

$$p = \frac{\left(\omega^4 + \omega^2\left(s_0 - b + agm_0 + Ba^2 s_0\right) + b\frac{s_0}{m_0} + gm_0 + as_0\right)\cos\omega\tau - k_0\omega\left(\frac{b}{m_0} + aBg + \left(\frac{1}{m_0} + a^2 B\right)\omega^2\right)\sin\omega\tau}{B(g + a\omega^2)}, \tag{44}$$

$$d = \frac{\left(\omega^4 + \omega^2\left(s_0 - b + agm_0 + Ba^2 s_0\right) + b\frac{s_0}{m_0} + gm_0 + as_0\right)\sin\omega\tau - k_0\omega\left(\frac{b}{m_0} + aBg + \left(\frac{1}{m_0} + a^2 B\right)\omega^2\right)\cos\omega\tau}{B\omega(g + a\omega^2)} \tag{45}$$

with $\omega \in \mathbb{R}^+$. Stability properties of the system depends on the dynamic properties of the accelerometer, which can be characterized by its natural frequency $\alpha_0 = \sqrt{s_0/m_0}/(2\pi)$. For large α_0, the system is unstable for any control gain parameters with finite NUR. The actual parameters of the accelerometer taken from [11] gives $\alpha_0 = 2$ kHz, for which model M4C2 is unstable. As α_0 is decreased, the NUR is also decreased, but the system remains unstable for any small α_0. A sample stability chart with the NURs can be seen in Fig. 8 for $\varepsilon = \frac{H}{2g}$, $\tau = 0.2$ s, and $\alpha_0 = 5$ Hz. It can be seen that the D-curves goes through the origin $(p, d) = (0, 0)$ and there is no region with zero NUR. Here, the NUR was determined using Stepan's formula [17]. For more technical details on these formulas see [18] and [19].

3.4.3 Model M4C3

Piecewise solution of Eq. (15) with (40), (41) and (9) with $r \geq 1$ and (4) over a sampling period gives the finite dimensional discrete map

$$\begin{bmatrix} \mathbf{x}_{j+1} \\ Q_j \\ Q_{j-1} \\ \vdots \\ Q_{j-r+1} \end{bmatrix} = \underbrace{\begin{bmatrix} \mathbf{P} & \mathbf{0}_{4\times1} & \dots & \mathbf{0}_{4\times1} & \mathbf{RB} \\ \mathbf{C}_4 & 0 & \dots & 0 & 0 \\ \mathbf{0}_{1\times4} & 1 & & 0 & 0 \\ \vdots & & \ddots & & \vdots \\ \mathbf{0}_{1\times4} & 0 & \dots & 1 & 0 \end{bmatrix}}_{\mathbf{\Phi}_{\text{M4C3}}} \begin{bmatrix} \mathbf{x}_j \\ Q_{j-1} \\ Q_{j-2} \\ \vdots \\ Q_{j-r} \end{bmatrix}, \tag{46}$$

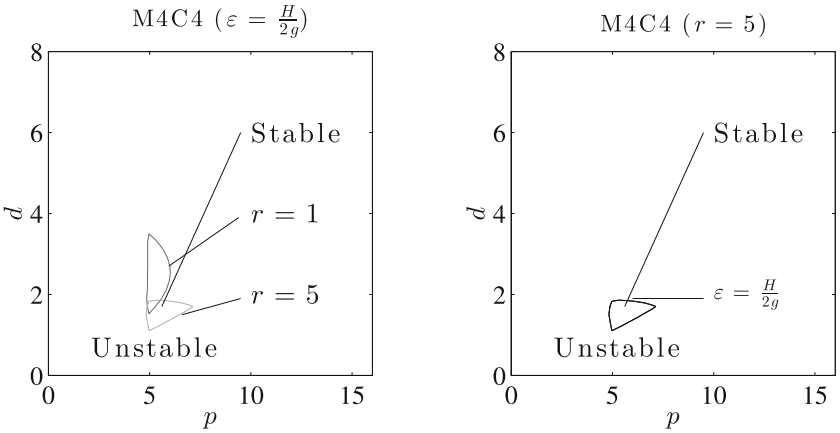

Fig. 10 Stability boundaries for M4C4 with $\tau = 0.2$ s

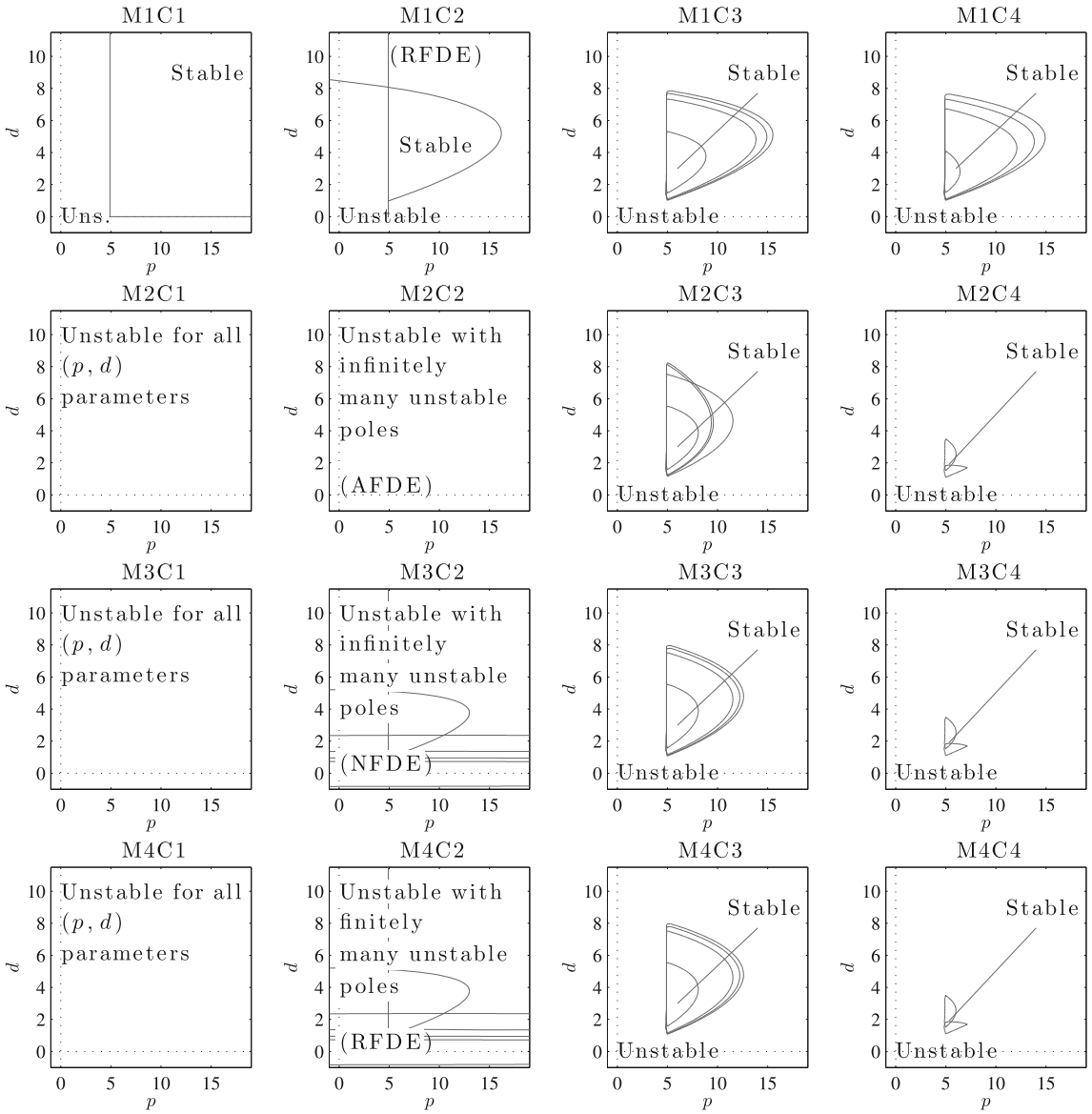

Fig. 11 Stability diagrams of the different models

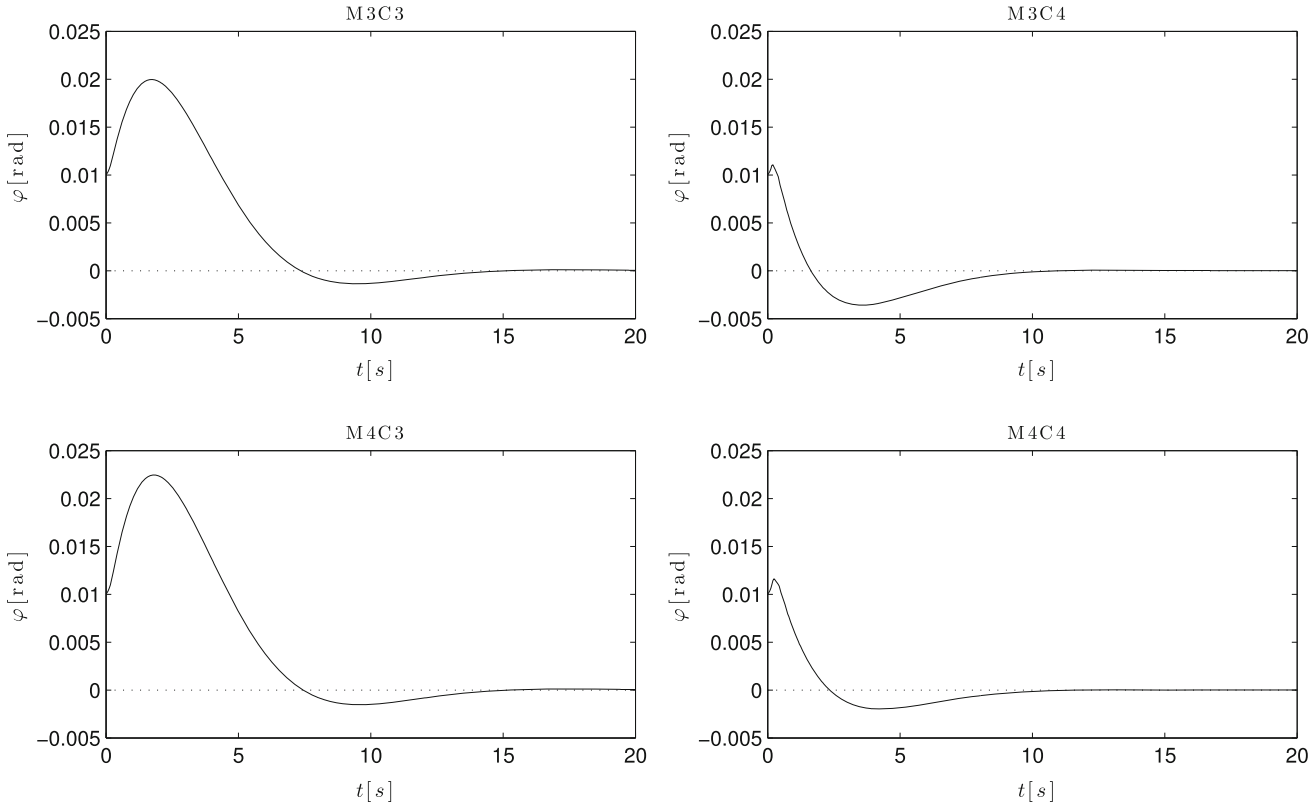

Fig. 12 Time histories for models M3C3, M3C4, M4C3, and M4C4 for $p = 5.1$, $d = 1.7$, $r = 5$ and initial condition $\varphi(\vartheta) = 0$ for $\vartheta \in [-\tau, 0)$ and $\varphi(0) = 0.01$ rad

where $\mathbf{P}$ and $\mathbf{R}$ are defined in (29) with (40) and (41) and

$$\mathbf{C}_4 = \begin{bmatrix} 0 & -p & 0 & -d \end{bmatrix}. \tag{47}$$

The stability of the system can be defined by the eigenvalues of the monodromy matrix $\mathbf{\Phi}_{\text{M4C3}}$. Some sample stability charts are presented in Fig. 9 for different ε, and for different r parameters.

3.4.4 Model M4C4

Equation (15) with (40), (41) and (10) with $r \geq 1$ and (4) induces the discrete map

$$\begin{bmatrix} \mathbf{x}_{j+1} \\ Q_j \\ Q_{j-1} \\ \vdots \\ Q_{j-r} \end{bmatrix} = \underbrace{\begin{bmatrix} \mathbf{P} & \mathbf{0}_{4\times 1} & \dots & \mathbf{R}\mathbf{B}K_1 & \mathbf{R}\mathbf{B}K_2 \\ \mathbf{C}_4 & 0 & \dots & 0 & 0 \\ \mathbf{0}_{1\times 4} & 1 & \dots & 0 & 0 \\ \vdots & & \ddots & & \vdots \\ \mathbf{0}_{1\times 4} & 0 & \dots & 1 & 0 \end{bmatrix}}_{\mathbf{\Phi}_{\text{M4C4}}} \begin{bmatrix} \mathbf{x}_j \\ Q_{j-1} \\ Q_{j-2} \\ \vdots \\ Q_{j-r-1} \end{bmatrix}, \tag{48}$$

where $\mathbf{P}$, $\mathbf{R}$ are defined in (29) with (40) and (41) and K_1 and $K2$ are given in (31) and $\mathbf{C}_4 = \begin{bmatrix} 0 & 1 & 0 & 0 \end{bmatrix}$. The stability of the system is determined by the eigenvalues of the monodromy matrix $\mathbf{\Phi}_{\text{M4C4}}$. Some stability charts are presented on Fig. 10 for different ε, and for different r parameters.

4 Comparison of the different models

Four different mechanical models (M1–M4) subjected to four different control concepts (C1–C4) were analyzed for the balancing task shown in Fig. 1. The main differences in the mechanical models is the model of the accelerometer, which is used to measure the angular position of the body to be balanced. The stability properties of the different modeling concepts were illustrated via stability diagrams in the plane of control parameters. A summary of the results are shown in Fig. 11. Each panel corresponds to one of the sixteen models. Models M1C1–M1C4 and M2C1–M2C4 were already investigated in [9]. An interesting feature is that a slight difference in the modeling concepts changes the dynamic behavior of the model radically. While model M2C1 cannot be stabilized for any control gain parameters and model M2C2 is unstable with infinitely many unsta-

ble characteristic roots, the introduction of sampling effect described by models M2C3 and M2C4 stabilizes the system. The main contribution of this paper is that the mechanical model is extended with a more detailed dynamic model of the accelerometer.

Models M4C1–M4C4 describes the accelerometer as an oscillator, while models M3C1–M3C4 neglects some terms in the modeling equations. Omission of further terms yields models M2C1–M2C4 and M1C1–M1C4. These models set up an interesting transition shown by the vertical columns in Fig. 11. The transition M1C1–M2C1–M3C1–M4C1 shows that, for control concept model C1, when the feedback delay is neglected ($\tau = 0$), only model M1 can be stabilized and models M2, M3 and M4 give unstable system for any control gain parameters.

An interesting transition between the models is given by the series M1C2–M2C2–M3C2–M4C2, which results in RFDEs, AFDEs and NFDEs of qualitatively different asymptotic properties. Model M1C2 is described by an RFDE, which can be stabilized by properly chosen control gains. Model M2C2 is governed by an AFDE, which is associated with infinitely many unstable characteristic roots independently on the control parameters. Model M3C2 is governed by an NFDE, which can be stabilized if the derivative control gain is less than a critical value otherwise the system is unstable with infinitely many unstable characteristic roots. Model M4C2 is described by an RFDE, but the system cannot be stabilized since any control gains combinations gives a system with finitely many unstable characteristic roots.

The stability diagrams for models M1C3–M4C3 and M1C4–M4C4 shows that the qualitative differences between the different mechanical models disappear when the sampling effect of the (digital) controller is involved into the model. For control concept model C4, when the digital effect is combined with a discrete calculation of the angular velocity, the stability diagrams for mechanical models M2, M3 and M4 are practically identical. This kind of stabilizing effect of the digital controller might be associated with the stabilizing effect of parametric forcing. This phenomenon is often demonstrated by the parametrically forced inverted pendulum, which is governed by the Mathieu equation (see, e.g., [12]). The piecewise constant state variable $\mathbf{x}(t_{j-r}) = \mathbf{x}(t_j - rh)$ over the interval $t \in [t_j, t_{j+1})$ can also be written as $\mathbf{x}(t-\rho(t))$, where $\rho(t) = rh + t - \mathrm{Int}(t/h)$ is a time periodic delay and Int denotes the integer part function. Thus, digital sampling actually introduces an h-periodic time delay, which is a kind of parametric forcing in the feedback delay.

In order to illustrate the stabilization of the digital effect, time histories are shown in Fig. 12 for models M3C3, M3C4, M4C3, and M4C4 with the same control gain parameters taken from the stable region and with same initial conditions. It can be seen that control concepts C4 have better performance with respect to overshoot and settling time.

In practice, different behavior of a real structure and its mathematical model is often attributed to the unmodeled dynamics or noise. In this paper, these unmodeled dynamics were partly modeled and their effect on the system behavior was analyzed for a simple balancing task. It was shown that slight modeling details may have a significant effect on the qualitative properties of the model for a given control concept model, but these differences vanishes when the sampling effect of the digital controller is involved into the model.

References

1. Hu HY, Wang ZH (2002) Dynamics of controlled mechanical systems with delayed feedback. Springer, Heidelberg
2. Kolmanovskii VB, Myshkis AD (1999) Introduction to the theory and applications of functional differential equations. Kluwer, Dordrecht
3. Hale JK, Lunel SMV (1993) Introduction to functional differential equations. Springer, New York
4. Niculescu S-I (2001) Delay effects on stability—a robust control approach. Springer, London
5. Xu Q, Stepan G, Wang Z (2017) Balancing a wheeled inverted pendulum with a single accelerometer in the presence of time delay. J Vib Control 23(4):604–614
6. Qin ZC, Li X, Zhong S, Sun JQ (2014) Control experiments on time-delayed dynamical systems. J Vib Control 20(6):827–837
7. Zhang XY, Sun JQ (2014) A note on the stability of linear dynamical systems with time delay. J Vib Control 20(10):1520–1527
8. Hajdu D, Insperger T (2016) Demonstration of the sensitivity of the Smith predictor to parameter uncertainties using stability diagrams. Int J Dyn Control 4(4):384–392
9. Insperger T, Wohlfart R, Turi J, Stepan G (2012) Equations with advanced arguments in stick balancing models. In: Time delay systems: methods, applications and new trends. Lecture notes in control and information sciences (LNCIS), vol 423. Springer, Berlin, pp 161–172
10. Gajamohan M, Muehlebach M, Widmer T, D'Andrea R (2013) The Cubli: a reaction wheel based 3D inverted pendulum. In: European control conference (ECC), 17–19, July 2013, Zürich, Switzerland, pp 268–274
11. Benevicius V, Ostasevicius V, Gaidys R (2013) Identification of capacitive MEMS accelerometer structure parameters for human body dynamics measurements. Sensors 13(9):11184–11195
12. Insperger T, Stepan G (2011) Semi-discretization for time-delay systems: stability and engineering applications. Springer, New York
13. Stepan G (2009) Delay effects in the human sensory system during balancing. Philos Trans R Soc A Math Phys Eng Sci 367:1195–1212
14. Habib G, Miklos A, Enikov ET, Stepan G, Rega G (2015) Nonlinear model-based parameter estimation and stability analysis of an aeropendulum subject to digital delayed control. Int J Dyn Control. doi:10.1007/s40435-015-0203-0
15. Habib G, Rega G, Stepan G (2016) Delayed digital position control of a single-DoF system and the nonlinear behavior of the act-and-wait controller. J Vib Control 22(2):481–495
16. Qin WB, Gomez MM, Orosz G (2017) Stability and frequency response under stochastic communication delays with applications

to connected cruise control design. IEEE Trans Intell Transp Syst 18(2):388–403
17. Stepan G (1989) Retarded dynamical systems. Longman, London
18. Xu Q, Wang ZH (2014) Exact stability test of neutral delay differential equations via a rough estimation of the testing integral. Int J Dyn Control 2(2):154–163
19. Xu Q, Stepan G, Wang ZH (2016) Delay-dependent stability analysis by using delay-independent integral evaluation. Automatica 70:153–157